Exploratory Search of New Magnetic Phases via Transition Metal Substitutions in $PtTe_2$

Undergraduate Research Thesis

Presented in Partial Fulfillment of the Requirements for graduation "with Honors Research Distinction" in the undergraduate colleges of The Ohio State University

By

Simo Kraguljac

The Ohio State University

April 2021

Project Advisor: Professor Joshua Goldberger, Department of Chemistry and Biochemistry

Table of Contents

Acknowledgements……iii

Vita……iv

List of Figures……v

Abstract……vi

Chapter 1: Introduction……1

Chapter 2: Search for Transition Metal Substituted $PtTe_2$……7

Chapter 3: $Cr_xPt_{1-x}Te_2$: Structure and Magnetism……11

Chapter 4: Exfoliation of $Cr_{0.45}Pt_{0.55}Te_2$……19

Chapter 5: Conclusions and Future Work……23

References……24

Acknowledgements

I would like to express my gratitude to all members of the Goldberger group who have helped me over the past few years of undergraduate research. I have received teaching and mentorship from everyone in the group who have helped me progress from learning basic techniques to being able to work on this thesis project. I would like to thank Ms. Yuxin Zhang of Professor ChunNing Lau's group for her help with AFM imaging. I would like to specifically thank Mr. Warren Huey who has been a mentor to me from the beginning of my time in the group and who has also contributed to this project. I would also like to thank Dr. Joshua Goldberger for his advising, support, and mentorship in my time in the research group. I am very thankful that I have had this opportunity to do meaningful undergraduate research.

Vita

Education

Brecksville-Broadview Heights High School……2017

The Ohio State University, Biochemistry……..2021

Honors and Awards

- Kraska Endowed Chemistry Scholarship (2019-2021)
- Raymond and Laura Goodrich Undergraduate Scholarship (2020-2021)

List of Figures

Figure 1. Pt-Te phase diagram[13]

Figure 2. Crystal Structures of $PtTe_2$, Pt_2Te_3, and Pt_3Te_4

Figure 3. Magnetic Ordering of CrI_3 in it's A) monolayer B) bilayer C) trilayer[14]

Figure 4. Degradation of CrI_3 under various conditions[15]

Figure 5. X-Ray Diffraction pattern of "VPt_2Te_4"

Figure 6. X-Ray Diffraction pattern of "$Mn_{0.25}Pt_{0.75}Te_2$" and "$Mn_{0.50}Pt_{0.50}Te_2$"

Figure 7. X-Ray Diffraction pattern of "$NiPt_2Te_4$"

Figure 8. X-Ray Diffraction pattern of $Cr_xPt_{1-x}Te_2$ ($0.05<x<0.45$)

Figure 9. Refined a lattice constant and interlayer spacing for $Cr_xPt_{1-x}Te_2$ ($0.05<x<0.45$)

Figure 10. Rietveld Refinement fitting of $Cr_{0.45}Pt_{0.55}Te_2$

Figure 11. $Cr_xPt_{1-x}Te_2$ shift in crystal structure 1T to 2T

Figure 12. A) Crystal data and Refinement results of $Cr_{0.45}Pt_{0.55}Te_2$ B) Atomic positions and thermal parameters

Figure 13. A) Chi vs T of powders B) Zero field cooled vs field cooled powder $Cr_{0.45}Pt_{0.55}Te_2$

Figure 14. Chi vs T curves of $Cr_{0.45}Pt_{0.55}Te_2$ crystal cross-plane and in-plane

Figure 15. Curie-Weiss fitting of $Cr_{0.45}Pt_{0.55}Te_2$ powder

Figure 16. Curie Weiss fitting data of $Cr_xPt_{1-x}Te_2$

Figure 17. M vs H Curves of $Cr_xPt_{1-x}Te_2$ powders

Figure 18. Exfoliation materials used, A) blue tape, B) Si/SiO_2 substrate

Figure 19. $Cr_{0.45}Pt_{0.55}Te_2$ exfoliation image: bilayer

Figure 20. $Cr_{0.45}Pt_{0.55}Te_2$ exfoliation image: 8 nm thick

Figure 21. $Cr_{0.45}Pt_{0.55}Te_2$ exfoliation image: 7 nm thick

Abstract

Two-dimensional (2D) magnetic materials is a very new field that has emerged in the last few years. 2D magnetism was previously not believed to be possible, but its discovery has opened up the field to find novel 2D magnets with interesting applications. Some of these applications include memory storage, sensors, and other sorts of devices. At this point, there are issues with many materials. The application of these materials is limited by a very low Curie temperature T_C or their propensity for oxidation, especially when exfoliated into very thin flakes. Here, we have explored the substitution of many transition metals into the $PtTe_2$ lattice, as this material is known to be a robust air-stable van der Waals material even in the monolayer form. Characterization of these materials was performed via X-Ray Diffraction. We have found that Ni, V, and Mn do not readily substitute with Pt in $PtTe_2$. On the other hand, up to 0.45 equivalents of chromium can substitute with Pt to form homogenous alloys of $Cr_xPt_{1-x}Te_2$ ($0.05<x<0.45$). Analysis of magnetic susceptibility in these powders shows a ferromagnetic ordering temperature that increases with increasing Cr substitution, and $Cr_{0.45}Pt_{0.55}Te_2$ has a T_C of 220K. We have been able to exfoliate the bulk materials into single-layer and few-layer flakes onto SiO_2/Si substrates which have been confirmed through atomic force microscopy (AFM) imaging. All of our synthesized $Cr_xPt_{1-x}Te_2$ materials have shown to be very air-stable, even upon exfoliation to few layers. Our results suggest that $Cr_xPt_{1-x}Te_2$ is a very promising layered magnetic material and may have potential in a variety of applications.

Chapter 1: Introduction

1.1: 2D Materials

The field of 2D materials largely began with the experimental discovery of graphene in 2004. Single-layer graphene was able to be isolated from bulk graphite by mechanical exfoliation onto a silicon wafer.[1] The work was rewarded with a Nobel Prize in Physics in 2010. The material was surprising for many reasons, mainly the stability of it in the monolayer and also the properties that it has which are much different than the bulk material. The honeycomb structure gave it electronic properties of a 2D semimetal with Dirac-cone like dispersions, which is much different than 3-dimensional graphite. It is extremely strong and highly conductive, having ultrahigh electron mobilities due to its unique electronic structure.[1] Many other interesting and unexpected properties have been studied in graphene, and these studies have opened up the search for more 2D materials that may have very interesting novel properties.[2-4] These unique properties have led to other promising applications, one of those being used as part of a chemical sensor device which has been shown to detect, NO_2, NH_3, and 2,4-dinitrotoluene.[5] Graphene and its derivatives have also been explored for application in ultracapacitors, various biomedical applications, and others.[6-7]

The discovery of graphene subsequently caused many other researchers to search for other 2D materials. Several others have been discovered, one of those being germanane (GeH), a graphane analog discovered in the Goldberger group. With a direct bandgap of 1.53 eV and much higher electron mobility than bulk Ge, this material also has promise in similar electronic devices.[8.]

Transition metal dichalcogenides (TMDs) are another large group of studied 2D materials with interesting properties. After graphene was discovered interest grew for TMDs. TMDs have

the formula MX_2 where M is a transition metal and X is a chalcogen (S, Te, Se). The monolayer is a hexagonal metal layer between chalcogens. They are generally semiconductors with a direct bandgap in a monolayer which is very different from the bulk. One example is MoS_2 which has a direct band gap of about 1.8 eV.[9] $NbSe_2$ and WTe2 are two other TMDs that show similar phenomena when exfoliated into a monolayer.[10-11] $PtTe_2$ is another TMD that has shown interesting properties. As platinum is a noble metal, the structure is very stable and remains stable when exfoliated to the monolayer. The nanosheets have shown conductivity up to 2.5 x 10^6 S/m and breakdown current density of 5.7 x 10^7 A/cm^2.[12] We believe we can utilize this stability to form stable monolayers of this material while incorporating transition metals to induce magnetism.

1.2. Structure and properties of $PtTe_2$

$PtTe_2$ has shown to be a very stable material even in its monolayer.[12] The phase diagram in Figure 1 shows the different species of Pt and Te.[13] This was the basis of our reasoning behind synthesis at 800 ºC as this is below where many transitions between the species $PtTe_2$, Pt_2Te_3, and Pt_3Te_4 take place. This will be discussed further in chapter 2. These crystal structures are shown in Figure 2. Pt_2Te_3 and Pt_3Te_4 both have a R-3m space group while $PtTe_2$ is a P-3m1 space group.

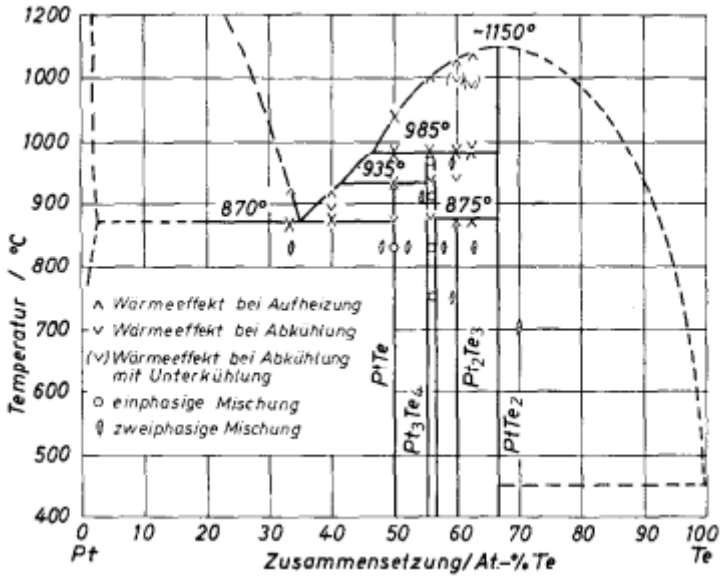

Figure 1. Pt-Te phase diagram.[13]

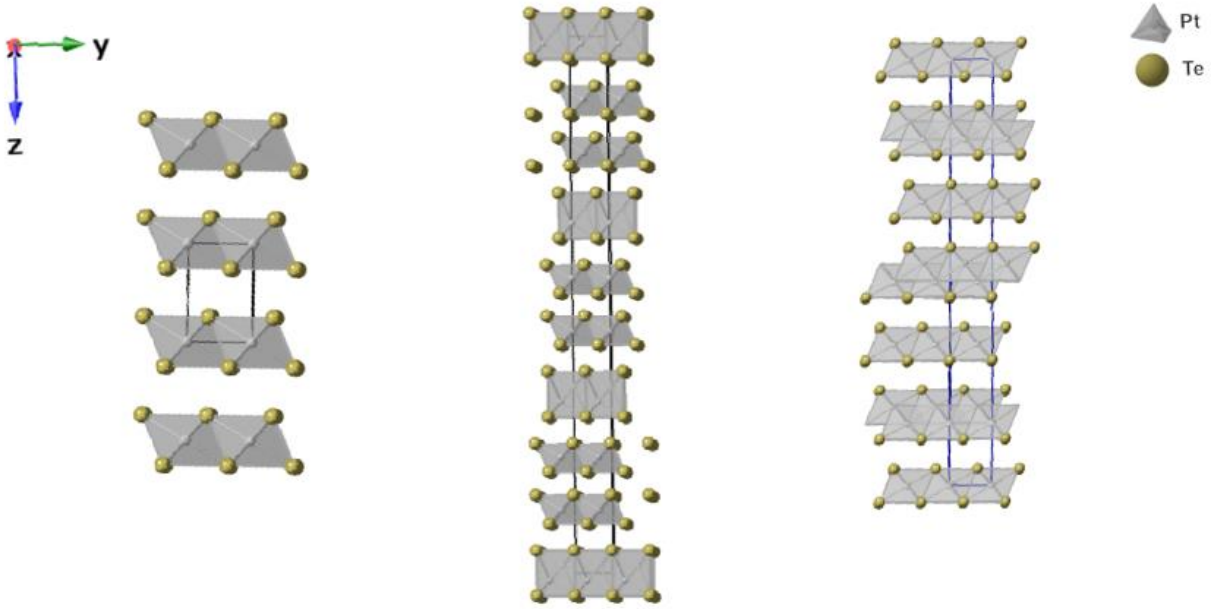

Figure 2: Crystal structures of $PtTe_2$, Pt_2Te_3, Pt_3Te_4 from left to right

1.3 2D Magnetic Materials

Although 2D material research had grown substantially, until recently it was believed that magnetism down to the monolayer was not believed to be possible. The Mermin-Wagner Theorem predicts that magnetic ordering is not possible in one and two dimensions at finite temperatures. However, magnetic anisotropy can open an excitation gap which allows for magnetism at finite Curie temperatures. The maintained magnetism was first observed in CrI_3, which sparked the field of 2D magnetism. They were able to mechanically exfoliate into few-layers and monolayers.[14] This material shows interesting magnetic behavior when exfoliated into thin layers. Figure 3a shows ferromagnetic behavior in monolayer CrI_3, while in the bilayer (Figure 3b) the material now exhibits antiferromagnetic behavior due to a cancelling of spins in the stacked layers. In Figure 3c, ferromagnetism reappears in the trilayer. This discovery was very important for the future of 2D magnets, however the application of CrI_3 is mainly limited by a low bulk Curie temperature of 61 K and a monolayer Curie temperature of 45 K. While it is promising that the monolayer has a Curie temperature that is only slightly lower than that of the bulk, it is important to find materials that maintain magnetism much closer to room temperature.[14] Another issue with these ultra-thin materials is stability. CrI_3 has shown to be very unstable when exfoliated into thin flakes, degrading quickly in various environments as shown in Figure 4.[15] These issues make CrI_3 and similar 2D magnets very difficult to be used in novel electronic devices. The instability and low Curie temperatures must be overcome in order to apply the new phenomenon of 2D magnetism to the future of electronics.

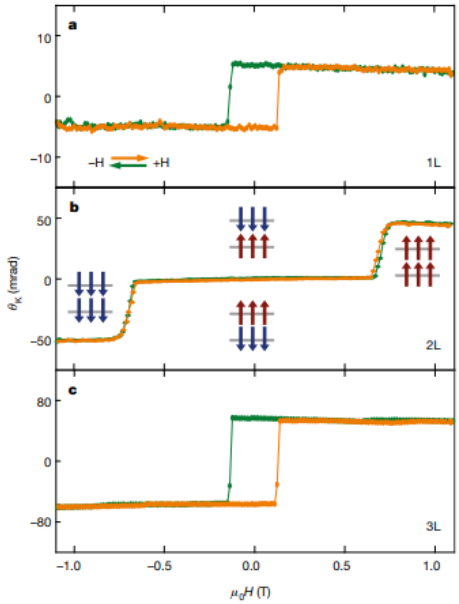

Figure 3: MOKE signal on a monolayer (1L) CrI_3 flake, showing hysteresis in the Kerr rotation as a function of applied magnetic field, indicative of ferromagnetic behaviour. **b**, MOKE signal from a bilayer CrI_3 showing vanishing Kerr rotation for applied fields ±0.65 T, suggesting antiferromagnetic behaviour. Insets depict bilayer (2L) magnetic ground states for different applied fields. **c**, MOKE signal on a trilayer (3L) flake, showing a return to ferromagnetic behaviour.[14]

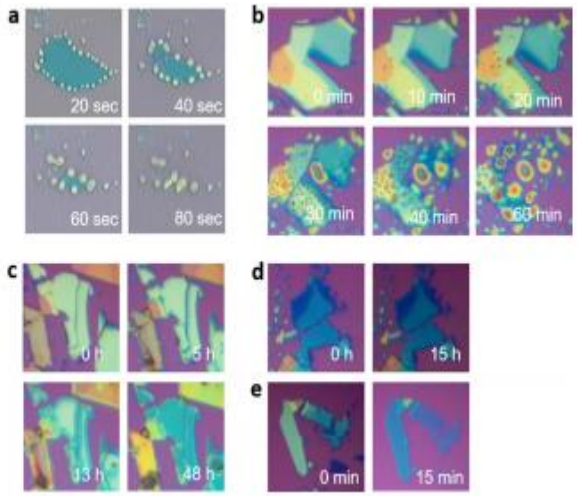

Figure 4: Degradation of CrI_3 a) air with light under microscope. b) Humid Argon. c) Air in the dark. d) Oxygen at room temperature e) Oxygen at 180 °C[15]

1.4 Transition Metal Substitution

One way some have explored to solve the problems of other 2D magnets is attempting transition metal substitutions into transition metal dichalcogenides (TMDs). Without transition metal doping these materials are nonmagnetic. Theoretical studies have shown that doping materials like MoS_2 with Mn, Fe, Co, etc. should be able to maintain ferromagnetic behavior up to room temperature.[16-18] Experiments have also indicated that some of these transition metal doped TMDs have the potential to maintain their magnetism to temperatures much higher than previously shown, which gives the materials wider applicability.[19] Magnetic moments have been seen up to around 3 bohr magnetons.[20] Generally, these systems have shown a lot of promise, but one problem is that many are not able to

substitute high levels of transition metals. Others have been able to synthesize these various systems with up to 10% transition metal substitution or less.[20-24]

Our motivation is to find air- and water-stable compounds that will display magnetism down to the monolayer limit. We aim to alloy the various platinum telluride phases with magnetic transition metals with the hope of incorporating large amounts of those transition metals in order to create materials with high Curie temperatures. This will be very useful in the future of electronic devices including sensors and memory storage.

Chapter 2: Search for Transition Metal Substituted $PtTe_2$

Our first goal was to identify which transition metals can substitute with Pt on the various Pt chalcogenide phases. Our general strategy was to first determine whether an alloy could form when various transition metals were substituted onto the lattice via the powder synthesis of MPt_2Te_4 (M=V, Mn, Ni, and Cr). If the transition metal dopant could substitute onto the Pt_3Te_4 lattice, significant changes in lattice constants would be expected. We began these initial experiments attempting to incorporate transition metals into Pt_3Te_4, however in almost all cases, we found that the $PtTe_2$ was formed.

To accomplish this synthesis, stoichiometric amounts of each element were combined in a small quartz tube inside of a larger quartz tube that was vacuum sealed. Synthesis of each powder sample was done with the same heating profile. These were all heated to 800 ºC over the course of 3 hours. This temperature was maintained for 7 days until cooling back to room temperature over the course of 60 hours. We explored substitution of Mn, Cr, V, and Ni as potential transition metal dopants. Some of these attempts were done early in our studies and the substitution was in Pt_3Te_4, but still gave valuable information on the potential of each dopant. In each attempt we look for a pure phase as well as significant peak shifting which indicates successful incorporation into $PtTe_2$.

First, observing the XRD of VPt_2Te_4 it is clear that impurities form and it also shows preference for $PtTe_2$. The most prominent impurity was V_3Te_4. Perhaps more importantly, there is very little to no apparent shift in peaks which would indicate that the vanadium has incorporated into this structure.

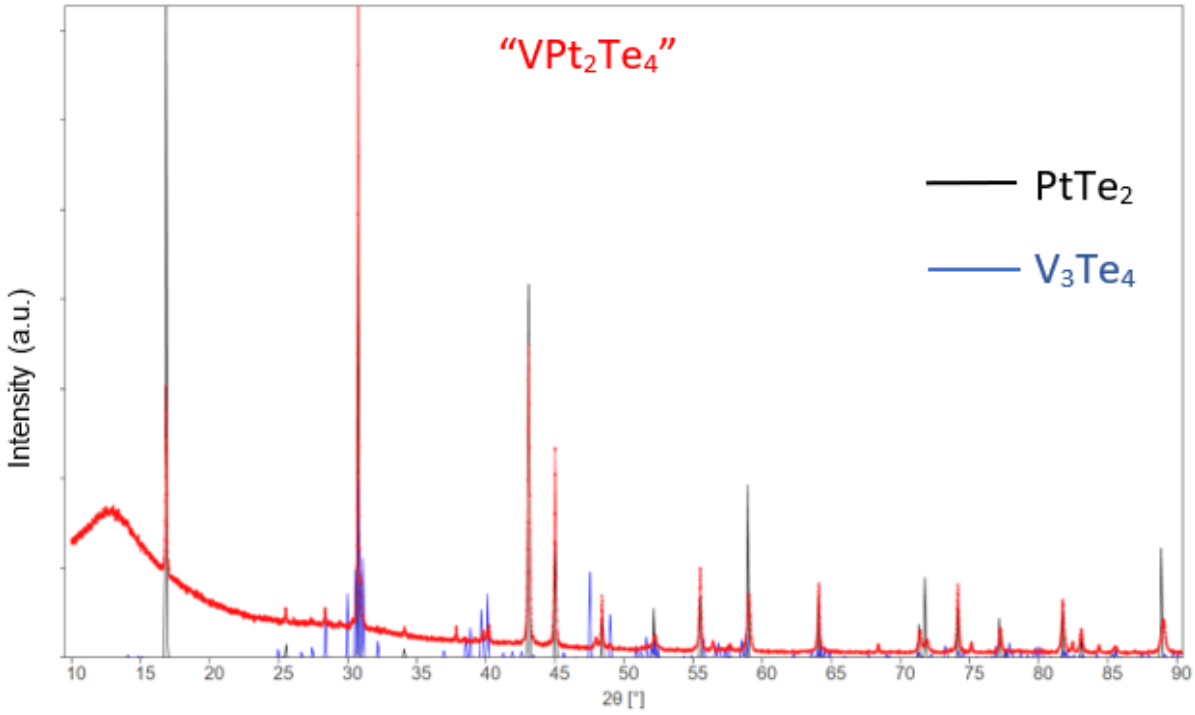

Figure 5: XRD pattern of product upon synthesizing "VPt_2Te_4". Calculated diffraction reflections corresponding to $PtTe_2$ are shown in black. No shift in the $PtTe_2$ diffraction reflections indicative of alloying is observed. Calculated V_3Te_4 diffraction reflections are shown in blue. This is the main observed impurity.

Next, we explored whether Mn could alloy in with $PtTe_2$. This material also does not show evidence of peak shifting. $Mn_{0.25}Pt_{0.75}Te_2$ and $Mn_{0.50}Pt_{0.50}Te_2$ were both synthesized and theoretically, peak shifts should be evident with increasing Mn content. This is not the case though as both XRDs are very similar. Significant impurities can be seen in the form of Te and $MnTe_2$.

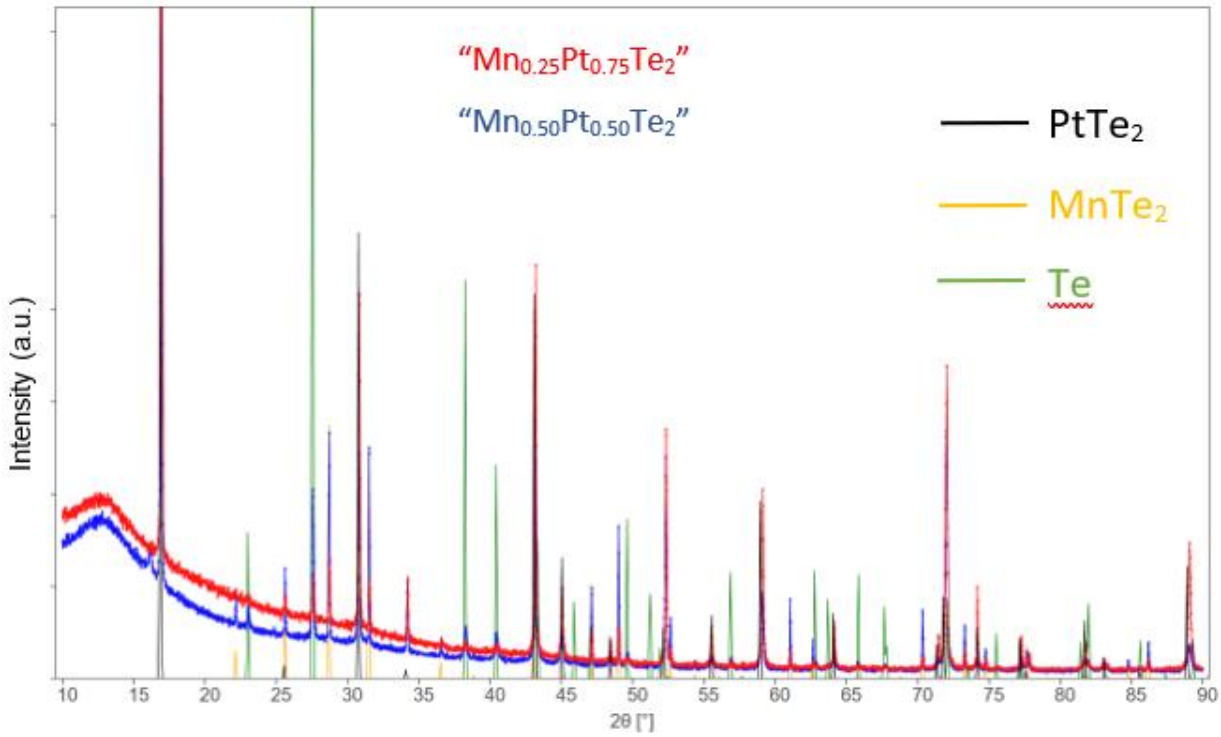

Figure 6: XRD pattern of product upon synthesizing "$Mn_{0.25}Pt_{0.75}Te_2$" and "$Mn_{0.50}Pt_{0.50}Te_2$." Calculated diffraction reflections corresponding to $PtTe_2$ are shown in black. No shift in the $PtTe_2$ diffraction reflections indicative of alloying is observed. Calculated $MnTe_2$ diffraction reflections are shown in yellow while Te are shown in green.

Finally, exploration of Ni substitution was unsuccessful as it did not show significant peak shifts indicating little substitution. This showed significant amounts of both $PtTe_2$ and Pt_3Te_4. The main impurity evident was $Ni_{2.60}Te_2$ Substitution of Chromium was successful and will be explored in Chapter 3.

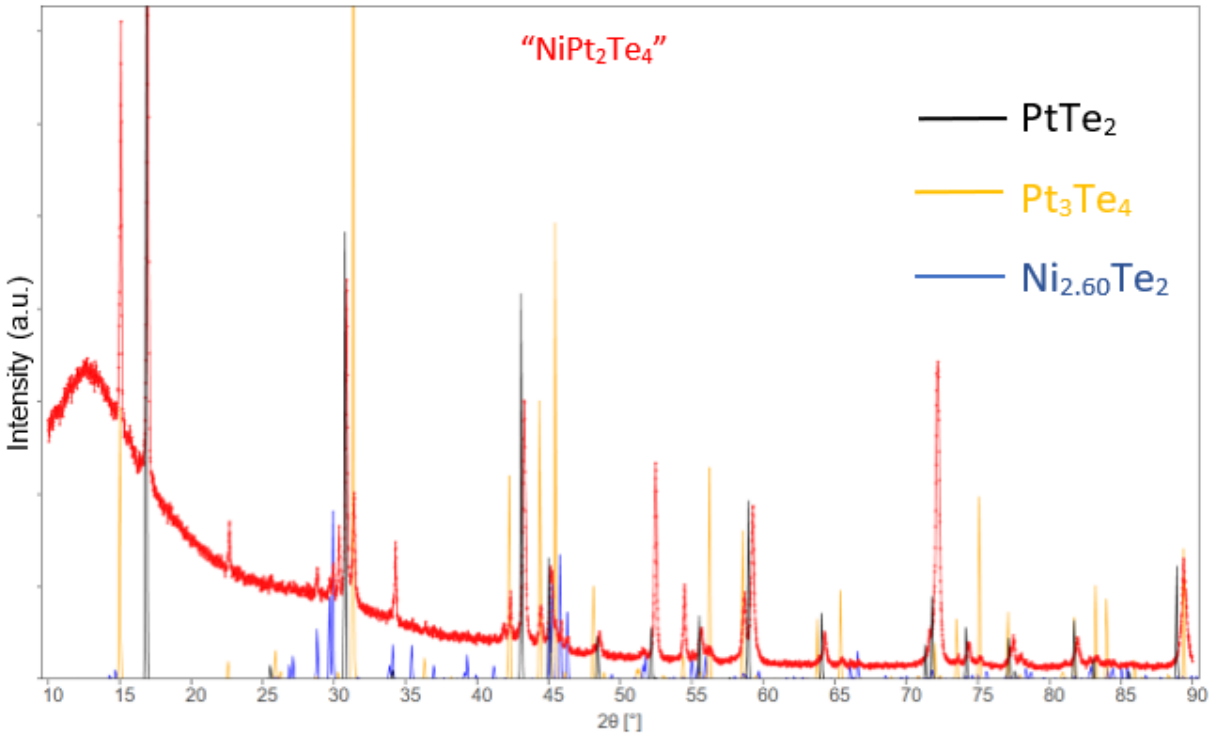

Figure 7: : XRD pattern of product upon synthesizing "$NiPt_2Te_4$". Calculated diffraction reflections corresponding to $PtTe_2$ are shown in black, Pt_3Te_4 are shown in yellow. No shift in the $PtTe_2$ or Pt_3Te_4 diffraction reflections indicative of alloying is observed. Calculated $Ni_{2.60}Te_2$ diffraction reflections are shown in blue.

Chapter 3: $Cr_xPt_{1-x}Te_2$

1.1 XRD of $Cr_xPt_{1-x}Te_2$

It was observed quickly that Cr clearly showed the most promise for substitution of the attempted transition metals. We were able to synthesize powders of $Cr_xPt_{1-x}Te_2$ where x ranged from 0.05 to 0.45. This is significant as many other TM doped systems at this point have not been able to incorporate nearly as much of the transition metal into their unit cell. XRD analysis showed that the c lattice had expanded from 5.224 Angstroms in $PtTe_2$ to roughly 5.4 Angstroms in $Cr_{0.25}Pt_{0.75}Te_2$. From here, we synthesized powders incorporating as much Cr as possible which ended up being 0.45 equivalents. We also then synthesized crystals of each Cr fraction using the same heating profile for the powders, but reaching a peak temperature of 1100ºC. $Cr_{0.05}Pt_{0.95}Te_2$ crystals could not be synthesized as we would need to reach temperatures higher than this, but this phase shows to be a poor magnet. Through analysis of Figure 8, a clear trend can be seen in that the 0 0 1 peak shifts left to a lower 2θ with increasing Cr content. A few of the phases show minimal Te impurity which can be seen most prominently at roughly 27 2θ. Further analysis indicates that with increasing Cr content, there is a clear trend of an increase in interlayer spacing and a decrease in the a lattice as shown in figure 9. Some single crystal

measurements have been done and they closely follow the powder trends for a lattice and interlayer spacing.

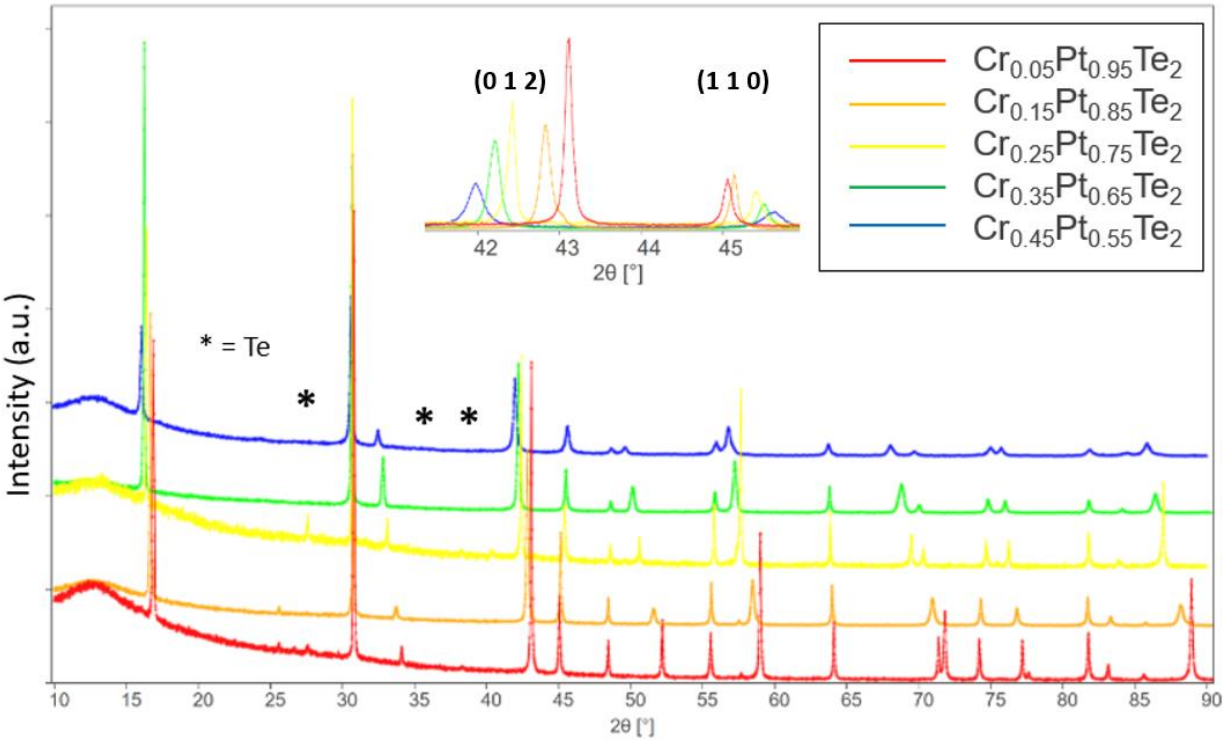

Figure 8: Full XRD plot of $Cr_xPt_{1-x}Te_2$. Inset indicates peak shifting of (0 1 2) and (1 1 0) peaks by chromium content.

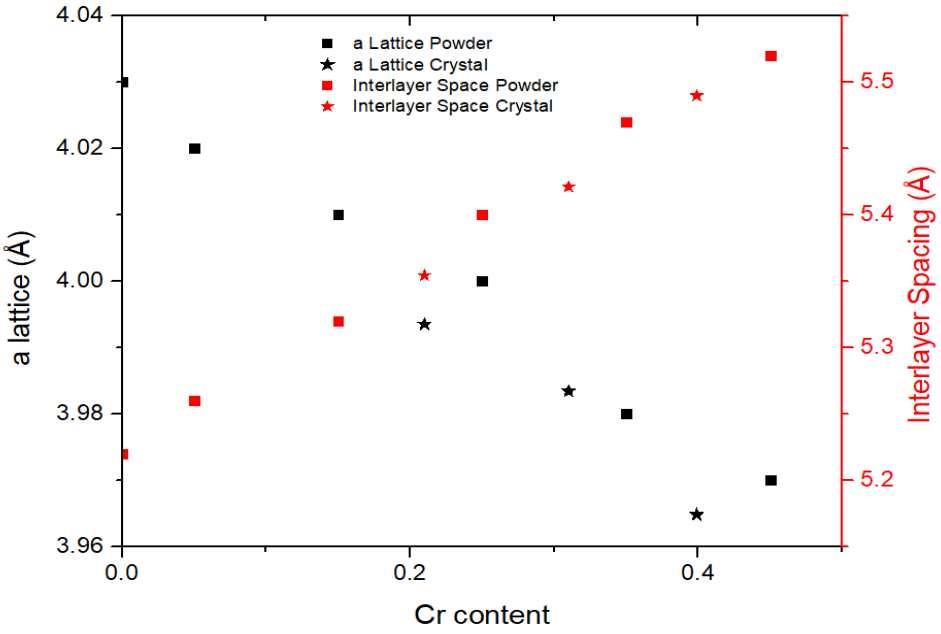

Figure 9: Refined a lattice constant, and interlayer spacing (c for 1T phase, c/2 for a 2T phase) for $Cr_xPt_{1-x}Te_2$ ($0<x<0.45$). Stars indicate single crystals. Squares indicate powders.

1.2 Rietveld Analysis

Rietveld Refinement was done with $Cr_{0.45}Pt_{0.55}Te_2$. Initially it was difficult to fit this, until we realized that this phase had a change in structure. The phases with lower chromium content have a 1T unit cell, while this phase has a 2T unit cell which is 2 layers. This is easily distinguished by the faint 001 peak at roughly 7 2θ as seen in figure 10. It is therefore determined that this unit cell shifts from 1T to 2T at some point between 0.35 and 0.45 equivalents of Cr. We were able to achieve close fitting with an Rwp value of roughly 5.039%. We also see an a lattice of roughly 3.97 Angstroms and a c lattice of 11.007 Angstroms. This c lattice is with the 2T unit cell, but when normalized to the other phases with a 1T unit cell it follows the trend shown in figure 6 closely. This shift in unit cell structure is shown in figure 11 as the unit cell shifts from a trigonal crystal structure, P-3m1 space group to a 2-layer trigonal crystal structure, maintaining the P-3m1 space group.

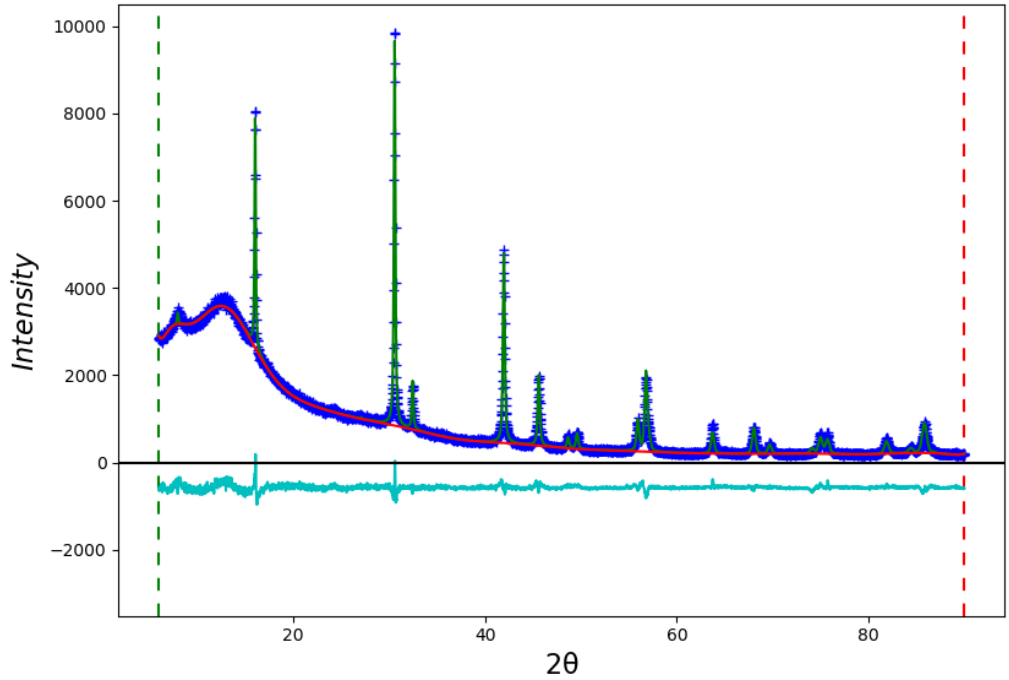

Figure 10: Rietveld Refinement fitting of $Cr_{0.45}Pt_{0.55}Te_2$

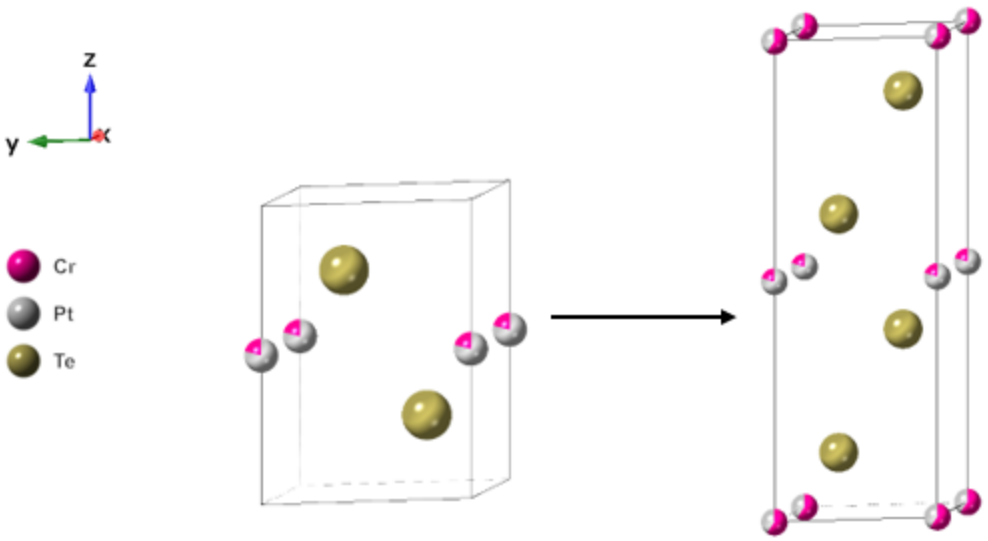

Figure 11: Shift in crystal structure of $Cr_x Pt_{1-x}Te_2$ from 1T to 2T

A

Space group	P-3m1
a (Å)	3.9705
c (Å)	11.0073
Z	2
wR	5.039
GOF	1.56
chi^2	9675.3

B

Atom	X	Y	Z	Fraction	U11	U33
Pt	0	0	0.5	0.782	0.035(8)	0.068(15)
Pt	0	0	0	0.537	0.019(9)	0.029(15)
Te	0.66667	0.33333	0.8711(8)	1	0.0211(15)	-0.0184(12)
Te	0.33333	0.66667	0.6321(8)	1	0.0211(15)	-0.0184(12)
Cr	0	0	0.5	0.218	0.035(8)	0.068(15)
Cr	0	0	0	0.463	0.019(9)	0.029(15)

Figure 12: A) Crystal data and refinement results of $Cr_{0.45}Pt_{0.55}Te_2$
B) Atomic positions and thermal parameters of $Cr_{0.45}Pt_{0.55}Te_2$

3.3: Magnetism

We have explored the magnetic properties of $Cr_xPt_{1-x}Te_2$. Because of our ability to incorporate large amounts of Cr we have seen ferromagnetic behavior in these powders up to roughly 220 K. The chi vs T curves in figure 13 demonstrate this. The Curie temperatures of the powders with low amounts of Cr are shown to be extremely low, meaning that these materials are not magnetic above temperatures near zero. A higher curie temperature is first seen in $Cr_{0.35}Pt_{0.65}Te_2$ which is above 100 K. The best magnet is $Cr_{0.45}Pt_{0.55}Te_2$. This material shows ferromagnetic behavior at higher temperatures which makes it promising for future electronics. The deviation in Figure 13b between zero field cooled and field cooled may indicate canting as spins do not show preference for realigning. This is demonstrated in figure 14 as well. This is not evident for the crystals in the in-plane direction, however, in the cross plane direction an even larger deviation can be seen. Figure 15 shows the Curie-Weiss fitting for zero field cooled $Cr_{0.45}Pt_{0.55}Te_2$ powder. Analysis shows the Curie Constant to be 3.98 K and the Weiss Constant to be 224.6 K. Other Curie-Weiss fitting results can be seen in figure 16. Figure 17 displays the ferromagnetic behavior of these powders as evidenced by the hysteresis in $Cr_{0.35}Pt_{0.65}Te_2$ and $Cr_{0.45}Pt_{0.55}Te_2$. Increasing chromium content translates into a stronger magnet as indicated in the plateau for $Cr_{0.35}Pt_{0.65}Te_2$ and $Cr_{0.45}Pt_{0.55}Te_2$ at roughly 1.5 and 2.25 bohr magnetons,

respectively. We hope and expect to see that upon further testing, this material will exhibit similar Curie temperatures down to ultrathin and monolayer limits.

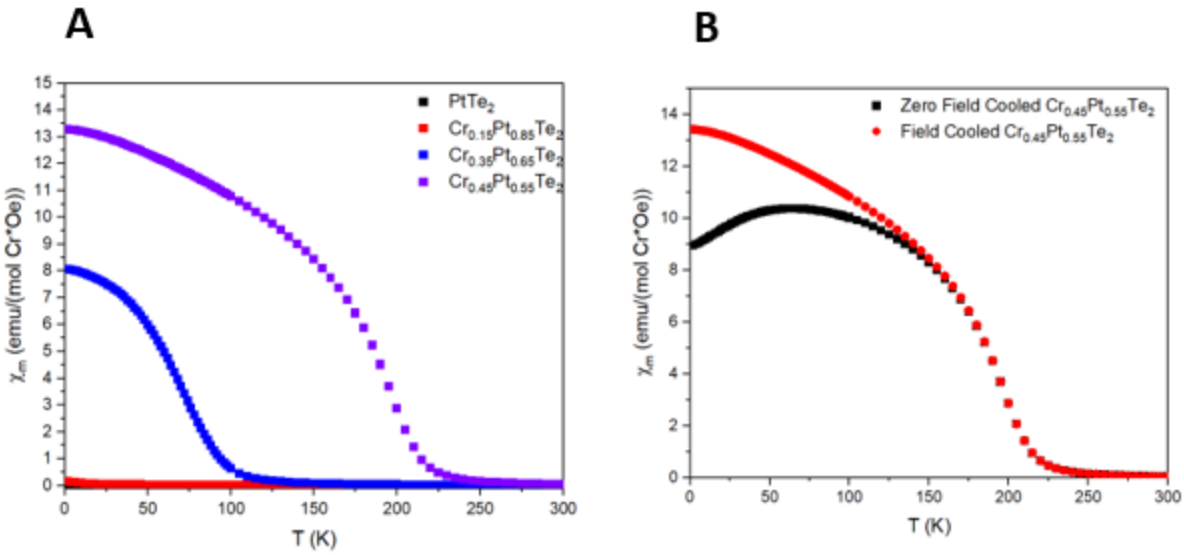

Figure 13: Chi vs T curves of $Cr_xPt_{1-x}Te_2$ powders. Magnetic susceptibility measurements all measured at 500 Orsted. B) zero-field cooled vs field cooled Chi vs T for $Cr_{0.45}Pt_{0.55}Te_2$ powder

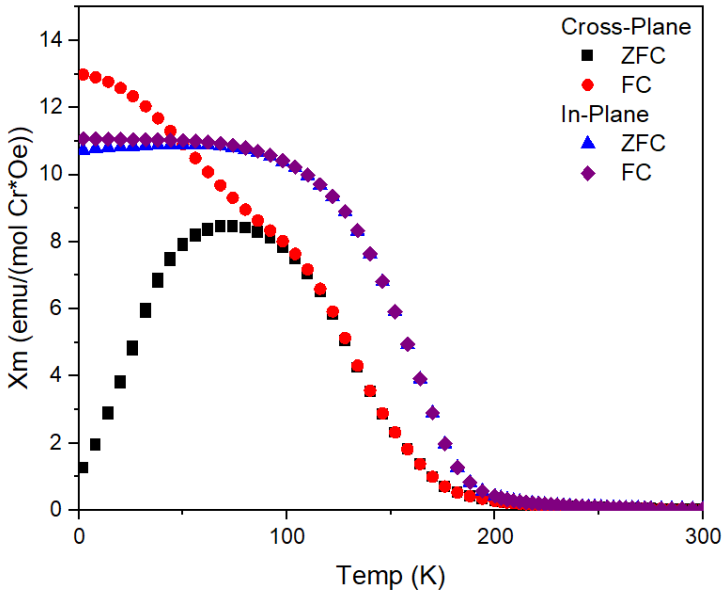

Figure 14: Chi vs T curves of $Cr_{0.45}Pt_{0.55}Te_2$ crystal. Zero-field cooled and field-cooled measurements taken in-plane and cross-plane

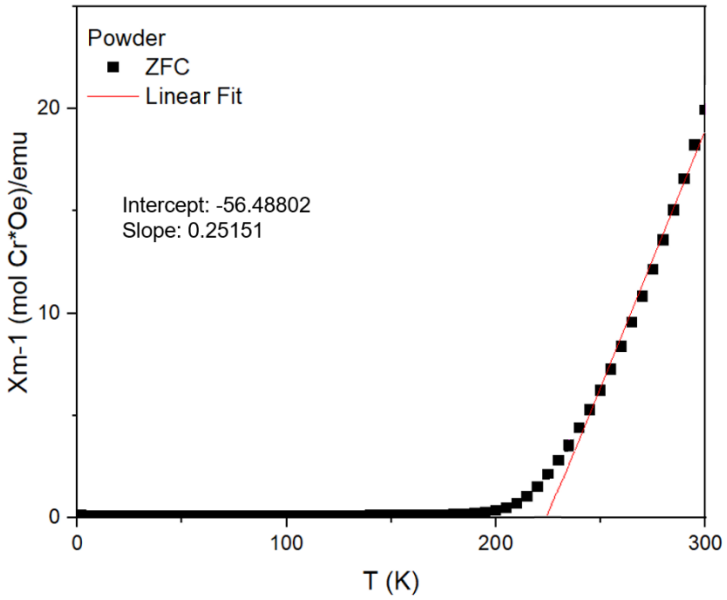

Figure 15: Curie Weiss fitting for zero field cooled $Cr_{0.45}Pt_{0.55}Te_2$ powder

Scan Type	Cr content	Sample Type	Curie Constant (K)	Weiss Constant (K)
ZFC	0.05	Powder	0.76	-4.5
ZFC	0.15	Powder	0.50	13.1
ZFC	0.25	Powder	1.59	59.8
ZFC	0.35	Powder	2.16	152.2
FC	0.35	Powder	2.16	152.5
ZFC	0.45	Powder	3.98	224.6
ZFC	0.45	In-plane	3.35	213.7
ZFC	0.45	Cross-Plane	3.14	210.0
FC	0.45	Powder	3.90	225.6
FC	0.45	In-Plane	3.38	213.1
FC	0.45	Cross-Plane	3.12	210.4

Figure 16: Curie Weiss fitting for $Cr_xPt_{1-x}Te_2$. Crystals measured in-plane and cross-plane

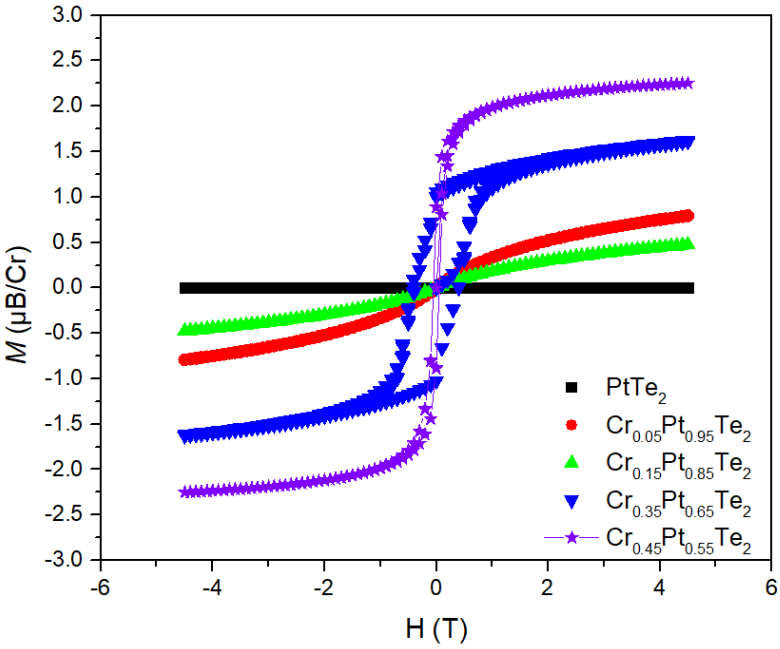

Figure 17: M vs H curves of $Cr_xPt_{1-x}Te_2$ powders

Chapter 4: Exfoliation of $Cr_{0.45}Pt_{0.55}Te_2$

Exfoliation of our materials is an important step that will make way for future work determining characteristics of $Cr_{0.45}Pt_{0.55}Te_2$ down to the monolayer limit. Our future goals include determining if it is air-stable when in monolayer form and to use it to understand how Tc changes with layer thickness in the future. Ultimately these materials could be utilized for different devices. It is notable that in contrast to other materials like CrI_3 we are able to observe under an optical microscope that our material does not show visible degradation for at least several weeks on a SiO_2/Si wafer.[15]

Our method of exfoliation includes multiple cleaning steps. First the substrate is cleaned by five-minute rinses of acetone, IPA, and acetone again. The wafer is then sonicated in a vial containing acetone for ten minutes. It is then sonicated again for an additional 10 minutes in IPA. The substrate is then rinsed with IPA and DI water before 10 minutes of plasma cleaning. The material is exfoliated by the tape method. A relatively small crystal is placed on the tape where it is repeatedly, mechanically thinned. The tape with the exfoliated crystals is then pressed onto the SiO_2/Si wafer and gently pressed onto it with a pencil eraser.

All $Cr_xPt_{1-x}Te_2$ ($0<x<0.45$) phases were found to readily exfoliate down to ~5-10 nm using this tape. Here we focus on the exfoliation of $Cr_{0.45}Pt_{0.55}Te_2$, since this phase has the highest T_C and is the most relevant for future applications. While we have not isolated large monolayers at this point, we have evidence that we can exfoliate this material down to a bilayer. It can be seen in figure 19 that on the top right corner of this flake, there is a small region that looks to be about 1 nm in height which indicates a bilayer since $Cr_{0.45}Pt_{0.55}Te_2$ has interlayer spacing of about 5.5 Å. This proves the existence and stability of $Cr_{0.45}Pt_{0.55}Te_2$ in its bilayer form and we hope to exfoliate larger monolayer sheets that will give way to more extensive

research. Figures 20 and 21 show larger flakes that were exfoliated from the same material and are less than 10 nm in thickness. The flake in figure 20 is roughly 8 nm in thickness while the one in figure 21 is roughly 7 nm in thickness. There is some residual tape residue on these flakes, and future methods will explore how to clean the substrate with the exfoliated flakes on it.

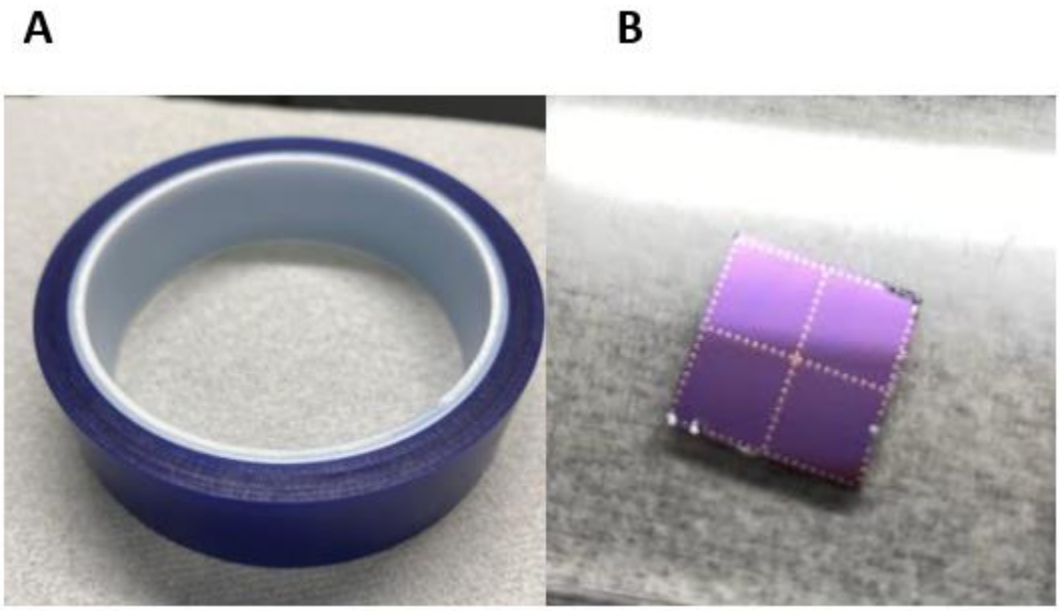

Figure 18: A) Blue tape used for mechanical exfoliation, B) single Si/SiO_2 substrate

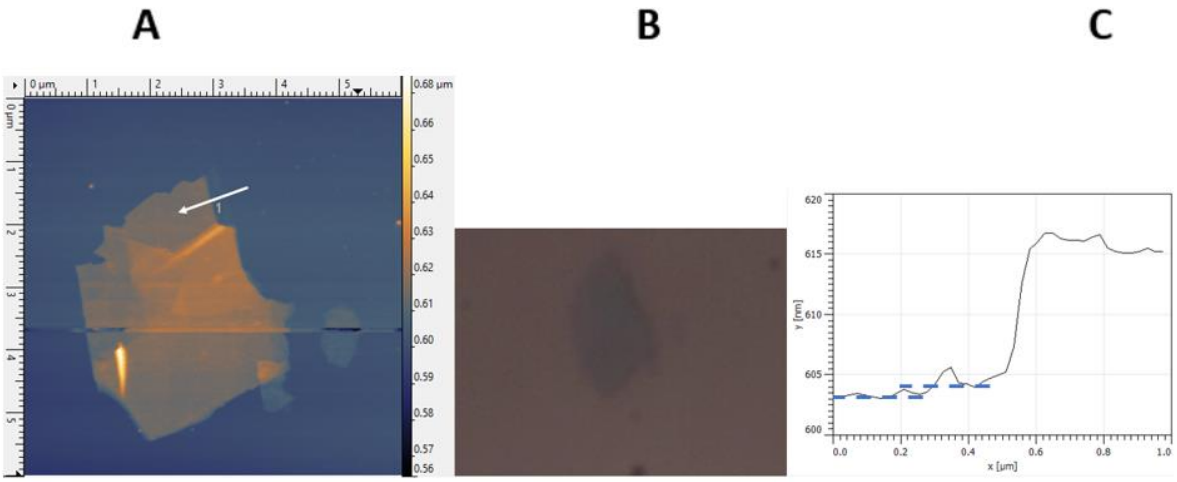

Figure 19: $Cr_{0.45}Pt_{0.55}Te_2$ exfoliation: a) AFM image of flake. B) flake on Si/SiO_2 substrate. C) depth measurement, roughly a 1 nm bilayer

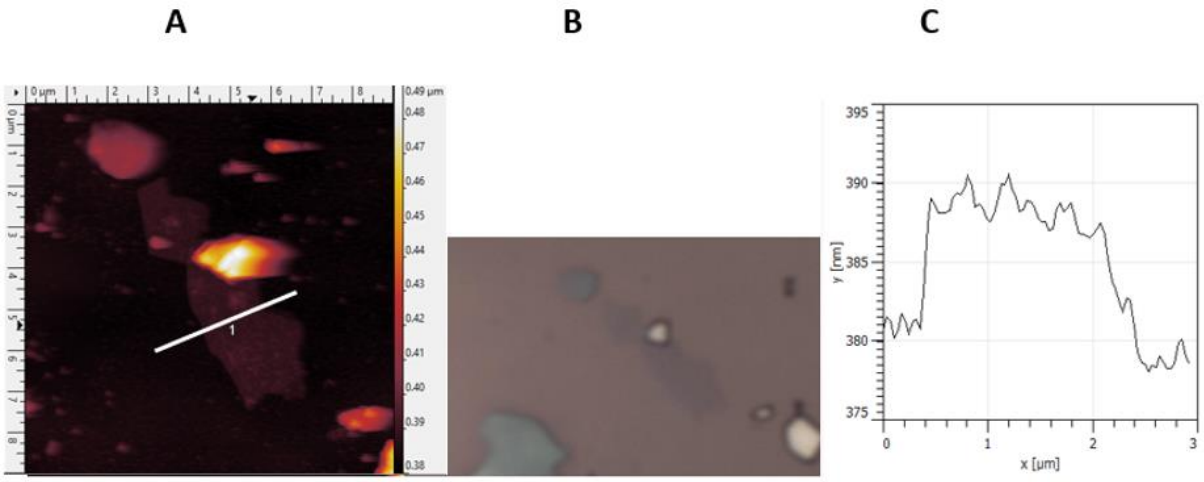

Figure 20: $Cr_{0.45}Pt_{0.55}Te_2$ exfoliation: a) AFM image of flake. B) flake on Si/SiO_2 substrate. C) depth measurement, roughly 8 nm

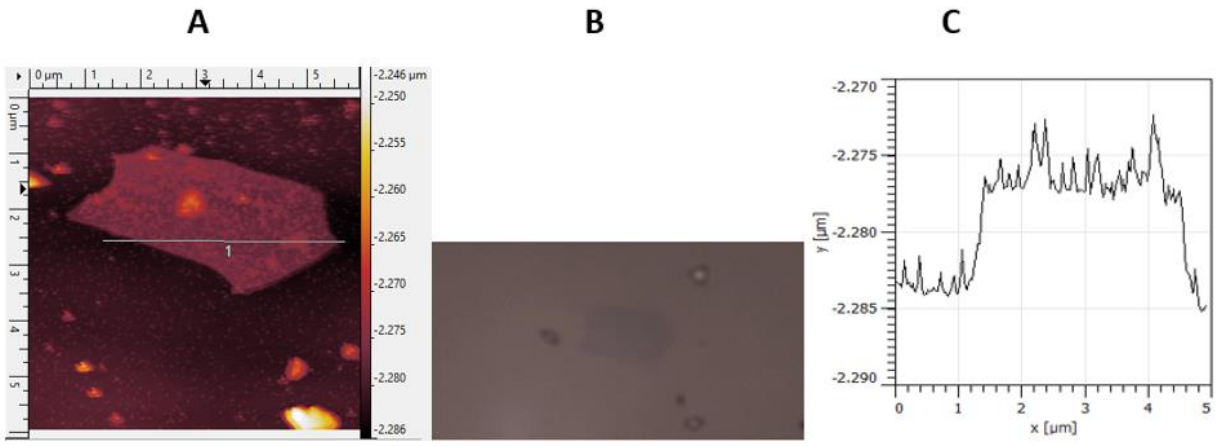

Figure 21: $Cr_{0.45}Pt_{0.55}Te_2$ exfoliation: a) AFM image of flake. B) flake on Si/SiO_2 substrate. C) depth measurement, roughly 7 nm

Chapter 5 Conclusions and Future Work

The field of 2D magnetism is expanding and we believe $Cr_x Pt_{1-x}Te_2$ is an important novel material with 2D magnetic properties. We have demonstrated the ability to substitute chromium into the $PtTe_2$ lattice up to 0.45 equivalents and form pure powders and crystals. The large amount of chromium is an improvement on other reported TMD doped systems. We have also found our material to have a Curie temperature of 220 K. We have demonstrated that our crystals can be exfoliated down to a few layers and have not shown any signs of degradation over an extended period of time. The lack of any visible degradation in bulk or exfoliated materials is a good sign for potential applications. Future work will be focused on optimization of exfoliation procedure in order to get larger few- and mono-layer sheets of our material. This will allow us to measure properties of the material at the monolayer level and see if there are significant changes from the bulk. We expect to see continued magnetic ordering up to a similar temperature to the bulk measurements. Our discovery of a new layered magnetic system that is very stable with high levels of incorporated transition metal is an important addition to the growing number of 2D magnetic materials.

References

1. Novoselov, K.S.; Geim, A.K.; Morozov S.V.; Jiang, D.; Zhang, Y.; Dubonos, S.V.; Grigorieva, I.V.; Firsov, A.A. Electric Field Effect in Atomically Thin Carbon Films. *Science*. **2004**, 306, 666-669.
2. Grigorenko, A.N.; Polini, M.; Novoselov, K.S. Graphene plasmonics. *Nature Photonics*, **2012**, 6, 749-758
3. Novoselov, K.S.; Geim, A.K.; Morozov, S.V.; Jiang, D.; Katsnelson, I. M.; Grigorieva, I.V.; Dubonos, S.V.; Firsov, A.A.; Two-dimensional gas of massless Dirac fermions in graphene. *Nature.* **2005**, 438, 197-200.
4. Bonaccorso, F.; Sun, Z.; Hasan, T.; Ferrari, A.C.; Graphene photonics and optoelectronics, *Nature Photonics*, **2010**, 4, 611-622.
5. Fowler, J. D.; Allen, M. J.; Tung, V. C.; Yang, Y.; Kaner, R. B.; Weiller, B. H. Practical Chemical Sensors from Chemically Derived Graphene. *ACS Nano.* **2009**, 3, 301–306.
6. Chung, C.; Kim, Y.K.; Shin, D.; Ryoo, S.R.; Hong; B.H.; Min, D.H. Biomedical Applications of Graphene and Graphene Oxide, *Acc. Chem. Res.* **2013**, 46, 2211-2224.
7. Stoller, M.D.; Park, S.; Zhu, Y.; An, J.; Ruoff, R.S. Graphene-Based Ultracapacitors. *Nano Lett.* **2008**, 8, 3498-3502.
8. Bianco, E.; Butler, S.; Jiang, S. S.; Restrepo, O. D.; Windl, W.; Goldberger, J. E. Stability and Exfoliation of Germanane: A Germanium Graphane Analogue. ACS Nano. **2013**, 7, 4414-21.
9. Mak, K.F.; Lee, C.; Hone, J.; Shan, J.; Heinx, T.F.; Atomically Thin MoS_2: A New Direct-Gap Semiconductor. *Physical Review Letters.*, **2010**, 105

10. Xi, X.; Zhao, L.; Wang, Z.; Berger, H.; Forro, L.; Shan, J.; Mak, K.F.; Strongly enhanced charge density wave order in monolayer $NbSe_2$. *Nature Nanotechnology*. **2015**, 10, 765-769
11. Ali, M. N.; Xiong, J.; Flynn, S.; Tao, J.; Gibson, Q.D.; Schoop, M.L.; Liang, T.; Haldolaarachchige, N.; Hirschberger, M.; Ong, N.P.; Cava, R.J.; **2014,** 514, 205-208.
12. Ma, H.; Chen, P.; Li, B.; Li, J.; Ai, R.; Zhang, Z.; Sun, G.; Yao, K.; Lin, Z.; Zhao, B.; Wu, R.; Tang, X.; Duan, X.; Duan, X.; Thickness-Tunable Synthesis of Ultrathin Type-II Dirac Semimetal $PtTe_2$ Single Crystals and Their Thickness-Dependent Electronic Properties., *Nano Letters*, **2018**, 18, 3523-3529.
13. Bhan, S.; Godecke, T.; Schubert, K.; Konstitution Einiger Mischungen Des Platins Mit B-Elementen (B = Sn, Sb, Te)., *Journal of the Less-Common Metals*, **1969**, 19, 121-140.
14. Huang, B.; Clark, G.; Navarro-Moratalla, E.; Klein, D.R.; Cheng, R.; Seyler, K.L.; Zhong, D.; Schmidgall, E.; McGuire, M.A.; Cobden, D.H.; Yao, W.; Xiao, D.; Jarillo-Herrero, P.; Xu, X. Layer-dependent ferromagnetism in a van der Waals crystal down to the monolayer limit. *Nature*., **2017**, 546, 270-273
15. Scherbakov, D.; Stepanov, P.; Weber, D.; Wang, Y.; Watanabe, K.; Taniguchi, T.; Hu, J.; Zhu, Y.; Mao, Z.; Windl, W.; Goldberger, J.; Bocrath, M.; Lau, C.N. Raman Spectroscopy, Photocatalytic Degradation and Stabilization of Atomically Thin Chromium Triiodide, *Nano Letters*, **2018**, 18, 4214-4219
16. Yue, Y.; Jiang, C.; Han, Y.; Wang, M.; Ren, J.; Wu, Y. Magnetic anisotropies of Mn-, Fe-, and Co-doped monolayer MoS_2. *Journal of Magnetism and Magnetic Materials*, **2020**, 496.

17. Jiang, C.; Wang, Y.; Zhang, Y.; Wang, H.; Qian, C.; Wan, J. Robust Half-Metallic Magnetism in Two-Dimensional Fe/MoS_2

18. Loh, L.; Zhang, Z.; Bosman, M.; Eda, G. Substiutional doping in 2d transition metal dichalcogenides. *Nano Research*. **2021**, 14, 1668-1681.

19. Fu, S.; Kang, K.; Shayan, K.; Yoshimura, A.; Dadras, S.; Wang, X.; Zhang, L.; Chen, S.; Liu, N.; Jindal, A.; Li, X.; Pasupathy, A.N.; Vamivakas, A. N.; Meunier, V.; Strauf, S.; Yang, E.; Enabling room temperature ferromagnetism in monolayer MoS_2 via in situ iron-doping. *Nature Communications.* **2020,** 11, 1-8.

20. Ahmed, S.; Ding, X.; Murmu, P.P.; Bao, N.N; Liu, R.; Kennedy, J.; Ding, J.; Yi, J.B; **2018** Magnetic properties of Co doped WSe2 by implantation, *J. Alloys Compd*., 731, 25–31.

21. Xia, B.; Guo, Q.; Gao, D.; Shi, S.; Tao, K.; High temperature ferromagnetism in Cu-doped MoS2 nanosheets *J. Phys. D: Appl. Phys*., **2016,** 49

22. Li, Q.; Zhao, X.; Deng, L.; Shi, Z.; Liu, S.; Wei, Q.; Zhang, L.; Cheng, Y,; Zhang, L.; Lu, H.; Gao, W.; Huang, W.; Qiu, C.; Xiang, G.; Pennycook, S.J.; Xiong, Q.; Loh, K.P.; Peng, B.; Enhanced Valley Zeeman Splitting in Fe-Doped Monolayer MoS_2. *ACS Nano*., **2020**, 14, 4636-4645.

23. Habib, M.; Muhammad, Z.; Khan, R.; Wu, C.; Ur Rehman, Z.; Zhou, Y.; Liu, H.; Song, L., **2018**, Ferromagnetism in CVT grown tungsten diselenide single crystals with nickel doping., *Nanotechnology*, 29

24. Kang, K.; Fu, S.; Shayan, K.; Anthony, Y.; Dadras,S.; Yuzan, X.; Kazunori, F.; Terrones, M.; Zhang, W.; Strauf, S.; Meunier, V.; Vamivakas, A.N.; Yang, E.; The effects of

substitutional Fe-doping on magnetism in MoS2 and WS2 monolayers, **2021,** *Nanotechnology*, 32